Characterization of Iron in Zeolites by X-band and Q-Band ESR, Pulsed ESR, and UV–Visible Spectroscopies

D. Goldfarb,† M. Bernardo, K. G. Strohmaier, D. E. W. Vaughan, and H. Thomann*,‡

Contribution from the Exxon Research and Engineering Company, Route 22 East, Annandale, New Jersey 08801

Received September 24, 1993®

Abstract: The local structure of Fe sites in a series of ferrisilicate and ferrialuminosilicate zeolites (Fe-sodalite (FeSOD), Fe-L (FeL), Fe-faujasite (FeFAU), FeZSM5, and Fe-mazzite (FeMAZ)) in which iron was incorporated during zeolite synthesis was studied by X- and Q-band ESR, electron spin echo detected ESR (ED-ESR), electron spin echo envelope modulation (ESEEM), and diffuse reflectance UV–vis spectroscopies. Samples were investigated as a function of Fe content and after variable-temperature dehydration and rehydration. Transitions characteristic of tetrahedrally coordinated Fe^{3+} were observed in the diffuse reflectance spectra of all Fe zeolites except for FeFAU. A strong $g = 2$ signal was observed in the ESR spectra for all the Fe zeolites whereas a $g = 4.3$ signal was observed only for the FeFAU, FeZSM5, and FeMAZ samples. Comparison between X- and Q-band spectra indicates that only one type of Fe^{3+} site is present in Fe-sodalite. Thus, neither the traditional assignment of the ESR signals of iron in the zeolite framework to a $g = 4.3$ signal nor some more recently proposed assignments could fully account for all the present results. We conclude that Fe^{3+} can be incorporated into framework sites in significant amounts in FeSOD, FeL, FeZSM5, and FeMAZ and probably also in FeFAU and that in each case framework Fe^{3+} exhibits a $g = 2$ ESR signal. Since extraframework Fe^{3+} can also show a $g = 2$ signal, its appearance does not provide evidence for framework substitution unless combined with other physical or chemical methods. Furthermore, the absence of the $g = 4.3$ signal in the ESR spectrum does not exclude the possibility of framework substitution in zeolites. Fe-faujasite was found to have significantly more extraframework Fe^{3+} than the other Fe zeolites studied. Combined ESR, ED-ESR, and ESEEM on Fe-faujasite that was subjected to dehydration/rehydration cycling show that phases with "aggregates" of Fe ions are generated either by dislodged framework Fe^{3+} and/or by migration of extraframework Fe^{3+}.

Introduction

The prospect of transition metal incorporation into the framework of aluminosilicate and aluminophosphate molecular sieves has drawn considerable interest in past years due to the potential new catalytic properties of the modified materials. These can be manifested in different acidities and in new catalytic activities based on the nature and loading of the incorporated transition metal ion and its influence on other metals present in the catalyst.

Iron exists as an impurity in several zeolites,[1,2] and it has been introduced in relatively large amounts during synthesis into a number of zeolites[3-10] and aluminophosphate molecular sieves (AlPO's).[11] A major problem in such materials is that the iron does not necessarily occupy exclusively framework sites. It can also exist as extraframework cations balancing the negative charge of the framework or as an interstitial phase of small particles located either within the molecular sieve cavities or in between the crystallites. In minerals such as clays, where iron is ubiquitous, it also exists as a surface coating or "staining".[12] Some of the techniques commonly used to characterize the iron sites include Mössbauer,[13] UV–vis, IR, and ESR spectroscopies.[14] More recently, extended X-ray absorption fine structure (EXAFS) spectroscopy has also been found to be very useful.[7-10] In spite of the diverse methods of characterization, the assignment and the identification of the framework iron is often ambiguous.

Since ferric iron is paramagnetic in both the low-spin and high-spin electronic configurations, ESR spectroscopy should be a good method for characterizing the iron sites in zeolites where the weak ligand field of the possible ligands (water, hydroxide, framework oxygen) results in high-spin ferric states. In this case, the interpretation of the ESR spectra is difficult due to complications associated with inhomogeneous broadening arising from the zero field splitting (ZFS) and overlapping signals. The X-band ESR spectrum of zeolites containing Fe^{3+} usually consists of three major signals at $g \approx 4.3$, $g \approx 2.2$–2.3, and $g \approx 2.0$. The commonly accepted assignment of these signals has been as follows: framework iron, iron in interstitial oxide or hydroxide phases, and iron in cation-exchange sites, respectively.[1,2,14] The appearance of a signal at $g \approx 4.3$ has often been used as evidence for framework substitution in zeolites and AlPO's.[3-5,14-20] Although used in many publications, the above assignment does

† On Sabbatical leave (until July 1993) from the Department of Chemical Physics, The Weizmann Institute of Science, Rehovot 76100, Israel.

‡ Also at Department of Chemistry, State University of New York, Stony Brook.

® Abstract published in *Advance ACS Abstracts*, May 15, 1994.

(1) McNicol, B. D.; Pott, G. T. *J. Catal.* **1972**, *25*, 223.
(2) Derouane, G. T.; Mestdagh, M.; Vielvoye, I. *J. Catal.* **1974**, *33*, 169.
(3) Zi, G.; Dake, T.; Ruiming, Z. *Zeolites* **1988**, *8*, 453.
(4) Kotasthane, A. N.; Shiralkar, V. P.; Hegde, S. G.; Kulkarni, S. B. *Zeolites* **1986**, *6*, 253.
(5) Inui, T.; Nagata, H.; Takeguchi, T.; Iwamato, S.; Matsuda, H.; Inoue, M. *J. Catal.* **1993**, *139*, 482.
(6) Lin, D. H.; Coudurier, G.; Vedrine, J. In *Zeolites: Facts, Figures, Future*; Jacobs, P. A., van Santen, R. A., Eds.; Elsevier Science Publishers B. V.: Amsterdam, The Netherlands, 1989; p 1431.
(7) Patarin, J.; Tuilier, M.; Durr, J.; Kessler, H. *Zeolites* **1992**, *12*, 70.
(8) Pickering, I. J.; Vaughan, D. E. W.; Strohmaier, K. G.; George, G. N.; Via, G. H. In *Proceedings of the 9th International Zeolite Conference*; von Ballmoos, R., Treacy, M. M. J., Higgins, J. B., Eds.; Butterworth/Heinemann: Stoneham, MA, 1993; p 197.
(9) Vaughan, D. E. W.; Strohmaier, K. G.; Pickering, I. J.; George, G. N. *Solid State Ionics* **1992**, *53–56*, 1282.
(10) Axon, S. A.; Fox, K. K.; Carr, S. W.; Klinowski, J. *Chem. Phys. Lett.* **1992**, *189*, 1.
(11) Flanigen, E. M.; Lok, B. M. T. K.; Patton, R. L.; Wilson, S. T. *Stud. Surf. Sci. Catal.* **1986**, *28*, 109.
(12) Jefferson, D. A.; Tricker, M. J.; Winterbottom, A. P. *Clays Clay Miner.* **1975**, *23*, 355.
(13) Berry, F. J. In *Mössbauer Spectroscopy Applied to Inorganic Chemistry*; Long, G. J., Ed.; Plenum Press: New York, 1984; Vol. 1, p 391.
(14) Ratnasami, P.; Kumar, R. *Catal. Today* **1991**, *9*, 328.
(15) Wichterlova, B. *Zeolites* **1981**, *1*, 181.
(16) Novalkova, J.; Kubelkova, L.; Wichterlova, B.; Tomas, T.; Dolejsek, Z. *Zeolites* **1982**, *2*, 217.
(17) Wichterlova, B.; Novakova, J.; Kubelkova, L.; Mikusik, P. *Zeolites* **1985**, *5*, 21.

0002-7863/94/1516-6344$04.50/0

not always agree with the results of other methods, raising questions regarding the validity of the assignment. For instance, Wenqin *et al.*[19] reported on the incorporation of Fe into the AlPO-5 framework, where they concluded from the Mössbauer results that the majority of the Fe^{3+} is tetrahedral and that a minor amount of the Fe^{3+} exists as nonframework octahedral Fe^{3+}. Electron probe microanalysis results also indicated that the majority of the Fe substituted for framework Al. The ESR spectrum, however, showed two signals, a strong one at $g = 2$ and a weaker one at $g = 4.3$. The latter was assigned to tetrahedral Fe without addressing the relative intensities of the two signals and their correspondence to the Mössbauer data. Recently Joshi *et al.*[20] reported the isomorphous substitution of Fe^{3+} into the LTL framework. The evidence for the presence of framework Fe was obtained from chemical analysis, framework IR, XPS, and Mössbauer data. The Mössbauer spectrum was assigned to a single Fe^{3+} site with an isomer shift expected for tetrahedral Fe^{3+}. The ESR spectrum, however, consisted of a major signal at $g = 2$ and a very weak $g = 4.3$ signal. Although inconsistent with the Mössbauer data interpretation, the authors used the existence of the weak $g = 4.3$ signal as supporting evidence for framework substitution. The traditional assignment of the Fe^{3+} signals in zeolites was challenged by Lin *et al.*,[6] who attributed the three signals to various types of framework sites, and by Park *et al.*,[21] who assigned the $g = 2$ signal of Fe in FAPO-5 to tetrahedral framework Fe^{3+} and the $g = 4.3$ signal to framework pseudo-octahedral ions. The above inconsistencies in the assignment of the ESR signals call for a reevaluation of the traditional assignment.

In the present paper we report on an investigation of a series of ferrisilicate and ferrialuminosilicate zeolites (Fe-sodalite, Fe-L, Fe-faujasite, FeZSM5, and Fe-mazzite) in which iron was incorporated, at both low and high levels, during zeolite synthesis. These zeolites were studied by UV–vis spectroscopy and by several ESR techniques: X-band and Q-band ESR spectroscopy, echo-detected (ED) ESR, and electron spin echo envelope modulation (ESEEM). We found that framework Fe^{3+} is not exclusively represented by a $g = 4.3$ signal but in fact in the zeolites studied exhibits a $g = 2$ signal. Furthermore, we demonstrate that signals due to extra framework Fe^{3+} can be identified by following the effects of thermal threatment by the combination of conventional ESR spectroscopy with pulsed ESR methods.

ESR Characteristics of Fe^{3+}. The spin Hamiltonian of low-spin Fe^{3+}, $S = {}^1/_2$, is dominated by the electronic Zeeman interaction with a highly anisotropic g factor. The ESR spectrum thus consists of a single transition, and in orientationally disordered samples it shows a characteristic powder pattern.[22] In contrast the the spin Hamiltonian of high-spin Fe^{3+}, (d^5, $S = {}^5/_2$) includes the ZFS interaction as well as the electron Zeeman interaction:[22,23]

$$H = g\beta\vec{B}_0\cdot\vec{S} + D\left[S_z^2 - \frac{1}{3}(S(S+1))\right] + E(S_x^2 - S_y^2) + \text{higher order terms}$$

In this case the g factor is isotropic and the ESR spectral characteristics are determined by the ZFS. The "higher order terms" originate from the cubic or lower symmetry of the crystal or ligand field and are generally assumed to be small compared to the quadratic terms. The ZFS parameters, D and E, are a measure of the deviation of the ion crystal field from ideal tetrahedral or octahedral symmetries for which both $D = 0$ and $E = 0$. When the reduced symmetry is axial, $D \neq 0$ and $E = 0$, while nonaxial symmetry results in $D \neq 0$ and $E \neq 0$. In the limit of rhombic symmetry, $E/D = 1/3$.

When the ZFS is small, namely $g\beta B_0 \gg D$, the five followed ESR transitions are well separated, all appearing around $g = 2$. All transitions, besides the $|-{}^1/_2\rangle \leftrightarrow |{}^1/_2\rangle$ transition show first-order dependence on the ZFS parameters and, in polycrystalline samples such as zeolites, will exhibit characteristic powder patterns whose width and shape depend on D and E. The $|-{}^1/_2\rangle \leftrightarrow |{}^1/_2\rangle$ transition depends on the ZFS only to second order, and therefore in polycrystalline materials its powder pattern is significantly narrower and dominates the ESR spectrum.[23,24] In this case, recording the ESR spectrum at higher microwave frequency, such as Q-band (34 GHz), is particularly advantageous, since the second-order broadening is significantly reduced, leading to higher spectral resolution.

The characteristics of the Fe^{3+} ESR spectrum in the case of a large ZFS, $g\beta B_0 \ll D$, were first analyzed by Castner *et al.*[25] When $E = 0$ the ESR spectrum consists of a broad powder pattern with singularities at $g = 6$ and $g = 2$. When $E/D = 1/3$, namely maximum rhombicity, the ESR spectrum consists of an isotropic signal at $g = 4.3$, originating from the middle Kramers doublet, and a broad feature at $g = 9$ due to the lowest Kramers doublet. A detailed discussion of the line shapes of these signals and their transition probabilities can be found in ref 26. It is important to note that in the case of a large ZFS the transition probabilities are highly anisotropic. Therefore the evaluation of the spin concentration from double integration of the ESR spectrum can lead to large errors, and it is necessary to numerically simulate the ESR spectrum for a quantitative measure of the spin concentration.[26]

Echo-Detected ESR. The echo-detected ESR (ED-ESR) spectrum is obtained by recording the electron spin echo intensity at a fixed echo delay time, τ, as a function of magnetic field. In principle the ED-ESR spectrum should correspond to the integral of the ESR spectrum where the latter is recorded under the conventional conditions of detecting the phase quadrature component of the first harmonic of the Zeeman field modulation frequency. In practice, under typical operating conditions, the use of Zeeman field modulation suppresses the signal intensity of very broad lines relative to that of more narrow line signals. In contrast, since no magnetic field modulation is used to record the ED-ESR spectrum, very broad line signals are readily detected.

One complication in the ED-ESR experiment is that the powder pattern envelope can be distorted if electron spin echo envelope modulation is observed. If this is the case, the shape of the ED-ESR powder pattern observed depends on the time interval τ of the spin echo pulse sequence.[27-29] In zeolites the nuclear modulation typically originates from framework ^{27}Al and from protons of water and hydroxyl groups. The modulation effect on the ED- ESR absorption envelope can be reduced or eliminated by recording spectra at several τ values and averaging the results or by recording the spectrum at a sufficiently long τ value so that the nuclear modulation amplitude has decayed to an insignificantly small value.

An additional complication occurs when several ESR signals with different phase memory times, T_m, contribute to the ED-ESR spectrum. The relative intensities of these signals will then depend on the values of τ and T_m. In this case the ED-ESR spectrum may be different from the usual ESR absorption spectrum. As we demonstrate in the present work, this can be

(18) Ojo, A. F.; Dwyer, J.; Parish, R. V. In *Zeolites: Facts, Figures, Future*; Jacobs, P. A., van Santen, R. A., Eds.; Elsevier Science Publishers B. V.: Amsterdam, The Netherlands, 1989; p 227.
(19) Wenqin, P.; Shilun, Q.; Qiubin, K.; Zhiyun, W.; Shaoyi, P. In *Zeolites: Facts, Figures, Future*; Jacobs, P. A., van Santen, R. A., Eds.; Elsevier Science Publishers B. V.: Amsterdam, The Netherlands, 1989; p 281.
(20) Joshi, P. N.; Awate, S. V.; Shiralkar, V. P. *J. Phys. Chem.* **1993**, *97*, 9749.
(21) Park, J. W.; Chon, H. *J. Catal.* **1992**, *133*, 159.
(22) Pilbrow, J. R. *Transition Ion Electron Paramagnetic resonance*; Clarendon Press: Oxford, U.K., 1990; p 125–144.
(23) Abragam, A.; Bleany, B. *Electron Paramagnetic Resonance of Transition Metal Ions*; Clarendon Press: Oxford, U.K., 1970; p 156–163.
(24) Meirovitch, E.; Poupko, R. *J. Phys. Chem.* **1978**, *82*, 1920.
(25) Castner, T.; Newell, G. W.; Holton, W. C.; Slichter, C. P. *J. Chem. Phys.* **1960**, *32*, 668.
(26) Yang, A.-S.; Gafney, B. J. *Biophys. J.* **1987**, *51*, 55.
(27) Mims, W. B.; Davis, J. L. *J. Chem. Phys.* **1976**, *64*, 3836.
(28) Goldfarb, D.; Kevan, L. *J. Magn. Reson.* **1988**, *78*, 276.
(29) Schweiger, A.; Ernst, R. R. *J. Magn. Reson.* **1988**, *77*, 512.

Table 1. Composition, Given in Relative Atomic Ratios, of the Zeolites Investigated

sample	zeolite	Fe	Al	Si	Na	K/TMA	Fe/(Fe + Al + Si)[a]	ref
FeFAU0	faujasite	0.00113	0.99887	2.75	0.95		0.03	41
FeFAU1	faujasite	0.00218	0.99782	2.79	0.96		0.06	36, 37
FeFAU2	faujasite	0.00257	0.99743	2.78	0.96		0.07	36, 37
FeFAU3	faujasite	0.00568	0.99432	2.72	0.96		0.15	36, 37
FeFAU4	faujasite	0.34	0.66	2.87	1.05		9.0	36, 37
FeMFI1	ZSM5	0.018	0.982	28.2	0.65		0.06	38
FeMFI2	ZSM5	0.992	0.008	27.91	0.79		3.4	38
FeSOD1	sodalite	0.001	0.999	0.96	1.32		0.05	9
FeSOD2	sodalite	0.989	0.01	5.15	0.082	0.91 (TMA)	16.0	39
FeMAZ1	mazzite	0.003	0.997	2.92	0.78		0.07	40
FeMAZ2	mazzite	0.05	0.95	3.23	0.765	0.23 (TMA)	1.2	40
FeLTL1	Linde L	0.002	0.998	2.71		1.01	0.07	8
FeLTL2	Linde L	0.27	0.73	2.94		1.11	6.6	8

[a] Molar ratio of Fe expressed as a molar percent.

an advantage, since T_m (and also T_1) "contrast" can be used to differentiate among overlapping signals by comparing ED-ESR spectra recorded at several τ values.

Electron Spin Echo Envelope Modulation (ESEEM). ESEEM is a pulsed ESR technique in which the electron spin echo intensity is recorded as a function of the time interval in a pulse sequence consisting of two or more short, intense microwave pulses.[30,31] An ESEEM spectrum analogous to the NMR spectrum of the paramagnetically coupled nuclei is obtained upon Fourier transformation (FT) of the ESEEM wave form. The ESEEM method is particularly suitable for the measurement of weak superhyperfine interactions of paramagnetic centers with surrounding nuclei.[31] In the case of zeolites containing paramagnetic transition metals, the ESEEM experiment can probe interactions of metal with ^{27}Al, ^{1}H, and possibly other exchange cations such as ^{23}Na, if present. In principle, in the case of a weak hyperfine interaction, where the modulation frequencies consist of only the Larmor frequency, ν_L, of the nucleus from which the modulation originates, the interaction distance and the number of interacting nuclei can be determined from the modulation depth.[31] This is practically applicable for $S = {}^1/_2$ and $I \geq {}^1/_2$, provided that the nuclear quadrupole interaction is negligible. In more complicated spin systems, such as Fe^{3+} with $S = {}^5/_2$ and ^{27}Al with $I = {}^5/_2$, the analysis of the ESEEM is significantly more complicated due to the presence of the ZFS[32,33] and nuclear quadrupole interactions,[34,35] which add a large number of unknown parameters to the analysis. Accordingly, in the present study we chose to use the ESEEM patterns on a comparative basis in order to probe for changes in the ^{27}Al and ^{1}H modulation patterns as an indication for variation in the local environment of the Fe^{3+} site.

Experimental Section

Zeolite Synthesis. Iron was added as $FeCl_3$ dissolved in water as the final component to the synthesis gels, partly replacing the desired level of Al^{3+} in otherwise conventional synthesis procedures. These procedures are described in detail in the references given in Table 1. Briefly, they comprised of dissolving $Al_2O_3 \cdot 3H_2O$ in a hot base solution (KOH, NaOH, or an alkylammonium hydroxide), adding the cooled aluminate solution to an aqueous silica (Dupont Ludox HS-40) or a sodium or potassium silicate solution in a small blender, and finally adding the ferric chloride solution. After thorough homogenization, the smooth gel was transferred to a Teflon bottle or autoclave (Parr acid digestion bomb) and heated at about 100 °C until crystallization was completed. In addition to the incorporation of Fe^{3+} into the "gel polymer" precursor, at higher iron loadings some iron was precipitated as a ferric hydroxide. Incorporation of the iron into the crystal structures results in white products. The synthesized zeolites were fully characterized by conventional X-ray diffraction methods using a Siemens D500 automated diffractometer. Apart from the sodalites (which are dense structures which do not sorb hexane), hexane sorption capacities confirmed the absence of significant pore blocking by precipitated Fe species. The zeolites studied, their compositions, and the abbreviations used in this paper are listed in Table 1.

Sample Preparation. Dehydration was performed by heating the as-synthesized zeolites in situ under vacuum to the desired temperature at a rate of 4 °C/min. The samples were then left at this temperature at a residual pressure of 1×10^{-4} Torr for 2–3 h, after which time they were sealed. Rehydration was carried out by breaking the sealed tube and placing it for several days at room temperature in a hydrator containing a saturated $Mg(NO_3)_2$ solution producing a 56% relative humidity.

ESR and Pulsed ESR Measurements. The X-band ESR (≈9.2) spectra were recorded on a Varian E-12 spectrometer both at room temperature and at 140 K. Q-band (≈34.0 GHz) ESR spectra were recorded at room temperature using a Bruker ESP300 spectrometer. The ESE (≈9.3) measurements were carried out at 1.2 K on a home-built spectrometer described elsewhere.[42] The ED-ESR spectra where obtained using the two-pulse sequence, $\frac{\pi}{2} - \tau - \pi - \tau - echo$, where τ was held constant, as a function of the external magnetic field.

Electron spin echo envelope modulation (ESEEM) wave forms were recorded using the two-pulse and three-pulse ($\frac{\pi}{2} - \tau - \frac{\pi}{2} - T - \frac{\pi}{2} - \tau - echo$) sequences where the echo intensity is measured as a function of the time intervals τ and T, respectively. Typically $\pi/2$ pulses of 30-ns duration where used.

Two-pulse FT-ESEEM spectra were obtained by reconstructing the missing data points of the ESEEM time domain wave form due to the spectrometer dead time using linear prediction (LP)[43] prior to Fourier transformation. The resulting time domain wave forms were then normaled to 1 at $\tau = 0$. The echo decay was then removed by a polynomial fit after which FT was performed without any further normalization. Accordingly, the peak intensities are proportional to the modulation amplitudes. The FTs of the ratioed three-pulse ESEEM were obtained without dead-time reconstruction.

UV–Visible Measurements. The UV–vis spectra of the as-synthesized zeolites were recorded on a Shimadzu UV-2101PC, diffuse reflectance spectrometer using a 2-nm slit width and a scanning rate of 2 nm/s.

Results

Diffuse Reflectance UV–Vis Measurements. The diffuse reflectance UV–vis spectra of the five high Fe content zeolites investigated are shown in Figure 1. FeSOD2 and FeMFI2 have very similar spectra with four lines at 373, 410, 436, and 480 nm

(30) Mims, W. B. *Phys. Rev. B* **1972**, *5*, 2409.
(31) Kevan, L. In *Time Domain Electron Spin Resonance*; Kevan, L., Schwartz, R. N., Eds.; Wiley: New York, 1979; pp 279–341.
(32) Coffino, A. R.; Peisach, J. *J. Chem. Phys.* **1992**, *97*, 3072.
(33) Larsen, R. G.; Halkides, C. J.; Singel, D. J. *J. Chem. Phys.* **1993**, *98*, 6784.
(34) Goldfarb, D.; Kevan, L. *J. Chem. Phys.* **1987**, *87*, 6323.
(35) Matar, K.; Goldfarb, D. *J. Chem. Phys.* **1992**, *96*, 6464.
(36) Vaughan, D. E. W. In *Microstructure and Properties of Catalysts*; Treacy, M. M. J., Thomas, J. M., White, J. M., Eds.; *Mater. Res. Soc. Symp. Ser.* **1988**, *111*, 89.
(37) Ratnasmy, P.; Kotasthane, A. N.; Shiralkar, V. P.; Thangaraj, A.; Ganapathy, S. In *Zeolite Synthesis*; Occelli, M. L., Robson, H. E., Eds.; ACS Symposium Series 398; American Chemical Society: Washington, DC, 1989; p 405.
(38) Kouwenhoven, H. W.; Stork, W. H. U.S. Patent 4,208,305, 1980.
(39) Szostak, R.; Thomas, T. L. *J. Chem. Soc., Chem. Commun.* **1986**, 113.
(40) Vaughan, D. E. W.; Strohmaier, K. G. U.S. Patent 5,185,136, 1993.
(41) Vaughan, D. E. W.; Edwards, C. G.; Barret, M. E. U.S. Patent 4,178,352, 1979.
(42) Thomann, H.; Bernardo, M. *Spectroscopy (Ottawa)* **1990**, *8*, 119. Thomann, H.; Bernardo, M. In *Methods Enzymol.* **1993**, *227*, 118.
(43) Barkhuijsen, H.; deBeer, R.; Bovee, W. M. M.; van Ormondt, D. *J. Magn. Reson.* **1985**, *61*, 465.

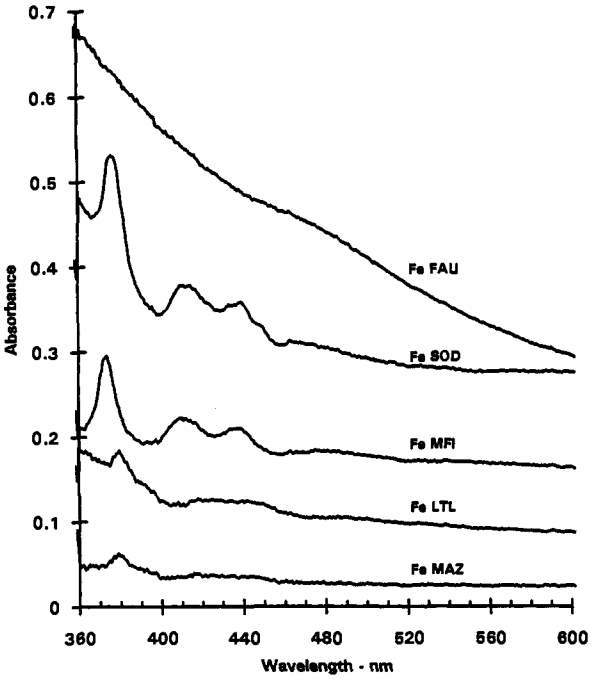

Figure 1. Diffuse reflectance UV–vis spectra of the high-level Fe zeolites FeFAU4, FeSOD2, FeMFI2, FeLTL2, and FeMAZ2.

and 376, 413, 438, and 480 nm, respectively, in good agreement with previously reported results in FeMFI.[6,7] Lin *et al.* assigned these peaks to weak "forbidden" d–d transitions from which they calculated the crystal splitting $10Dq$. The value of $10Dq$ was found to be similar to that of $FePO_4$, where the Fe^{3+} is tetrahedral, and was significantly smaller than that of Fe^{3+} in octahedral fields. Accordingly the authors concluded that the optically active Fe^{3+} site has tetrahedral symmetry.

FeLTL2 and FeMAZ2 exhibit spectra similar to those of FeSOD2 and FeMFI, with peaks at 386, 392, 423, 443, and 485 nm and 378, 392, 416, and 444 nm, respectively. The peak intensities are weaker than those in the spectra of FeSOD2 and FeMFI2 and are somewhat shifted to lower frequencies. Moreover, the resolution is reduced and the appearance of the shoulder at 392 nm suggests the existence of two sets of lines. The peak intensities roughly correlate with the Fe content, with FeLTL2 being an exception. Unlike the other zeolites investigated, the FeFAU4 spectrum is comprised of a significantly more intense high-frequency charge-transfer band[6] which masks the d–d transitions, if present. We note also that while all other samples were essentially white, FeFAU4 was tan.

ESR Measurements. The X-band ESR spectra of the zeolites with the high Fe contents, FeLTL2, FeSOD2, FeMFI2, FeFAU4, and FeMAZ2, recorded at room temperature and at 140 K are shown in Figure 2. While the spectra of FeMAZ2, FeFAU4, and FeMFI2 show the three signals usually observed in Fe containing zeolites at $g = 4.3$, $g = 2.2$–2.3, and $g = 2.0$, the spectra of FeLTL2 and FeSOD2 (ferrisilicate sodalite) consist of a single peak at $g = 2.0$, though a close observation reveals a very weak signal at $g = 4.3$ in the spectrum of FeLTL2. The spectra recorded at room temperature and at 140 K are rather similar. The main difference is the lower relative intensity of the $g = 4.3$ signal in the room temperature spectra which may be an indication of a faster spin relaxation. A comparison of the signal intensity in the FeSOD2 with that of $FePO_4$, which also has a single $g = 2$ line, showed that the $g = 2$ signal accounts for the majority of the iron in the FeSOD2 sample.

The Q-band spectra of these zeolites recorded at room temperature are shown in Figure 3A. All spectra show only one signal at $g = 2$. The most plausible reasons that the $g = 4.3$ and $g = 2.3$ signals are not observed in the Q-band spectra are excessive broadening by frequency-dependent relaxation mechanisms[44] or that the condition $g\beta B_0 \ll D$ is no longer valid at Q-band. If D becomes comparable to the electron Zeeman interaction at 34 GHz (1.1 cm^{-1}), significant broadening of the $g = 4.3$ peak would be expected. In either case, in the absence of these signals the width and the shape of the $g = 2$ signal is better determined.

The line widths of the $g = 2$ signals are significantly smaller in the Q-band spectra compared to the X-band spectra as shown in Table 2. This narrowing indicates that the length width is at least partially due to the second-order broadening of the $|-1/2\rangle \leftrightarrow |1/2\rangle$ transition, which is proportional to $D^2/(g\beta B_0)$. If the broadening mechanisms were limited to the ZFS only, a narrowing given by the ratio (3.7) of the spectrometer frequencies at Q- and X-band is expected, since the second-order broadening is inversely proportional to $g\beta B_0$. Inspection of Table 2 shows that this is not the case; the narrowing is smaller than expected, suggesting the existence of other sources of broadening. Possible sources of broadening include overlapping spectra of different species, spin–spin interactions which are effective at high Fe concentrations, and frequency-dependent relaxation mechanisms.

In order to eliminate potential broadening of the ESR signals due to spin–spin interactions, we examined samples with very low Fe loadings, (<0.1%). The X-band spectra of the FeMAZ1, FeMFI1, and FeFAU1 exhibit the same signals as a those of the corresponding samples with the high Fe loadings. The relative intensities of the signals within a given spectrum are, however, a function of the Fe content. The relative intensity of the $g = 4.3$ signal is larger in the spectra of the samples with the low Fe loadings. The largest difference is observed in FeLTL, as shown in Figure 4, where at high Fe loadings (sample FeLTL2) the $g = 4.3$ signal is hardly detectable whereas in the low Fe sample, FeLTL1, its intensity is comparable to that in the other zeolites. The Q-band spectra of the low Fe content samples are shown in Figure 3B. Note the significant decrease in the line widths for all five zeolites as expected. The widths of the $g = 2$ signals in the X- and Q-band spectra of these samples are compared in Table 2.

The spectra of both the ferrisilicate sodalite (high Fe, FeSOD2) and the aluminosilicate sodalite (low Fe, FeSOD1) are unique in the sense that in both samples the $g = 4.3$ signal is negligible. The X-band spectra of FeSOD1 recorded at room temperature, shown in Figure 5A, and at 140 K are practically identical and consist of two components, one narrow and one broader, at $g = 2$. We assign the narrow signal, which is also observed in the spectra of all other zeolites with low Fe loadings and corresponds to a very low spin concentration, to an "impurity". We assign the broader line at $g = 2$ to the $|-1/2\rangle \leftrightarrow |1/2\rangle$ ESR transition of the high spin Fe^{3+}. The spectra also exhibit a broad shoulder on both the low- and high-field sides of the $g = 2$ signal. The low-field signal at $g = 2.32$ is better resolved while the high-field shoulder is partly buried under the center line. These broad components can be assigned to singularities in the powder patterns of the $|-5/2\rangle \leftrightarrow |-3/2\rangle$, $|-3/2\rangle \leftrightarrow |-1/2\rangle$, $|1/2\rangle \leftrightarrow |3/2\rangle$, and $|3/2\rangle \leftrightarrow |5/2\rangle$ ESR transitions which depend to first order on D and E. In this case the signal originates from a single Fe^{3+} site. Alternatively it is possible that the broad components arise from the $|-1/2\rangle \leftrightarrow |1/2\rangle$ ESR transition of another Fe^{3+} species with a different set of ZFS parameters. The X-band spectrum alone cannot distinguish between the above two possibilities. However,

(44) Alpert, Y.; Couder, Y.; Tuchendler, J.; Thome, H. *Biochim. Biophys. Acta* **1973**, *322*, 34.
(45) McCracken, J.; Peisach, J.; Dooley, D. M. *J. Am. Chem. Soc.* **1987**, *109*, 4064.
(46) Mims, W. B.; Davis, J. L.; Peisach, J. *Biophys. J.* **1989**, *45*, 755.
(47) Mombourquette, M. J.; Tennant, W. C.; Weil, J. A. *J. Chem. Phys.* **1986**, *85*, 68.
(48) Choi, D.; Weil, J. A. *Phys. Rev. B* **1990**, *42*, 9759.
(49) Minge, J.; Mombourquette, M. J.; Weil, J. A. *Phys. Rev. B* **1990**, *42*, 33.
(50) Minge, J.; Weil, J. A.; McGavin, D. G. *Phys. Rev. B* **1989**, *40*, 6490.
(51) Hulliburton, L. E.; Hantehzadeh; Mombourquette, M. J.; Weil, J. A. *Phys. Rev. B* **1989**, *40*, 2076.

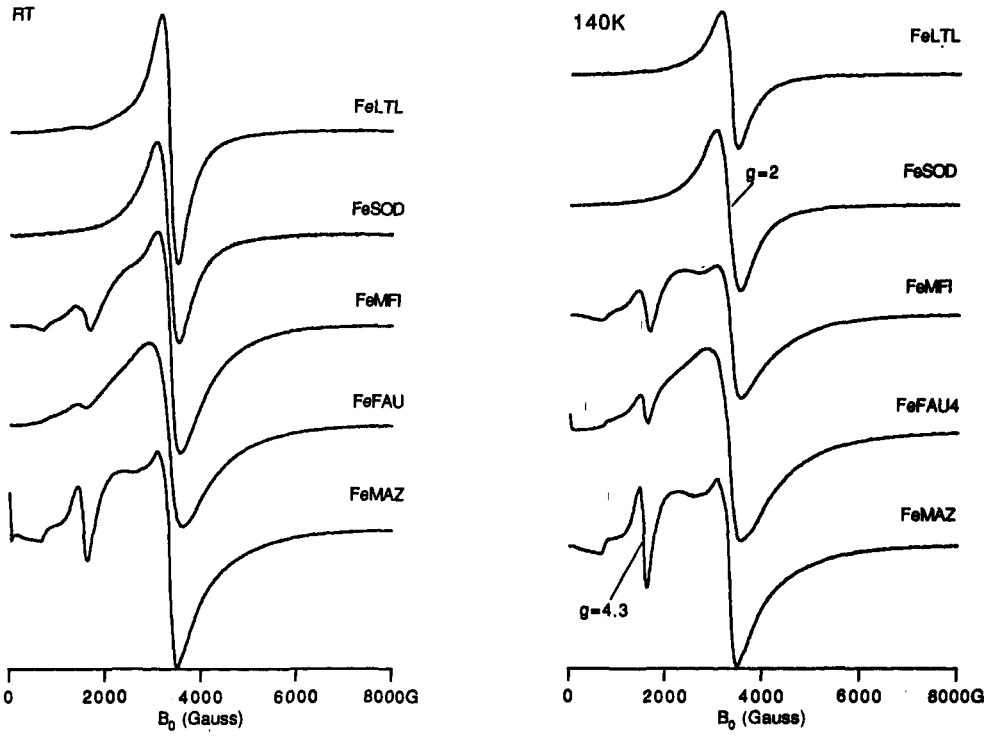

Figure 2. X-Band ESR spectra of the high-level Fe zeolites FeLTL2, FeSOD2, FeMFI2, FeFAU4, and FeMAZ2 recorded at 296 K (left side) and at 140 K (right side).

a comparison of the relative position of the two signals in the X- and Q-band spectra can provide the answer. In the Q-band spectrum, shown in Figure 5B, the two shoulders are better resolved but their positions relative to the center of the spectrum remain unchanged. This excludes the possibility that the shoulders can be assigned to the $|-^1/_2\rangle \leftrightarrow |^1/_2\rangle$ ESR transition of another Fe^{3+} species, since the splitting between the shoulders would be frequency dependent. Therefore, we assign the center $g = 2$ peak and the shoulders to a single Fe^{3+} species with a D value in the range of a few hundred gauss. In comparing the X- and Q-band ESR spectra, note also the narrowing of the center $|-^1/_2\rangle \leftrightarrow |^1/_2\rangle$ transition by a factor of 3.4 (from 156 g to 46 G), which is very close to the expected value (3.7).

In order to establish the assignment of the ESR signal from the extraframework Fe^{3+} cations, FeLTL2 was exchanged with 1 wt % Fe^{3+}. The X-band ESR spectrum of the exchanged sample showed a broadening of the $g = 2$ signal and practically no change in the weak $g = 4.3$ signal. A similar experimental performed with NaY containing Fe^{3+} impurities and an exchange level of about 0.05 wt % gave significantly different results. The exchange generated a new sharp signal superimposed on the previous broader $g = 4.3$ signal.

ESE Measurements: Dehydration/Rehydration Studies. The FeFAU4 sample was unique among the zeolite samples studied. No d–d transitions in the 300–500-nm region were observed in the UV–vis spectrum, and its ESR spectra exhibited larger line widths (see Figure 3). The FeFAU4 sample also had a more pronounced tan color than the other samples. Therefore, it is reasonable to suspect that it contains significant amounts of extraframework Fe. In order to test this hypothesis, information on the Fe^{3+} surroundings in the FeFAU sample is required. Such information can be observed from electron spin echo (ESE) experiments.

ESE experiments can be performed only on paramagnetically diluted samples in which the spin–spin interactions are minimized. This is required in order to achieve spin relaxation times long enough so that electron spin echoes can be detected. ESR spectra of FeFAU were therefore examined as a function of Fe loading, as shown in Figure 6, in order to establish whether the ESR signatures of the Fe were the same at lower and higher Fe loading. The sample that was synthesized without intentional iron addition still shows an Fe^{3+} signal and was found to contain 0.03% Fe (see Table 1). This is due to the presence of Fe in the silica and alumina starting materials. For Fe loading up to 0.07%, the $g = 4.3$ signal increases more rapidly than the $g = 2$ signal, whereas further increase in the Fe content results in a significantly larger increase in the $g = 2$ and $g \approx 2.3$ signals. We take the appearance of the same signals at low and high Fe contents as evidence for the presence of the same types of Fe species in the low- and high-loaded samples. The relative amounts of the different Fe^{3+} species, however, do vary with Fe content. The best ESE results in terms of S/N were obtained for the sample with 0.07% Fe (FeFAU2). Thus the ESE experiments reported below were performed on this sample.

A particularly useful methodology for assigning the ESR signals of the Fe^{3+} (or other paramagnetic transition metal ions) in the zeolite is the investigation of dehydration and rehydration in conjunction with ESR and ESE experiments. Figure 7A shows the X-band ESR spectra of the as-synthesized FeFAU2 sample along with those of samples dehydrated at 398 and 673 K. After dehydration, the $g = 2$ signal broadens and appears weaker than the $g = 4.3$ signal.

The apparent decrease in the intensity of the $g = 2$ signal after the mild dehydration conditions may arise from broadening induced by an increase in D. It is also possible that the $g = 2$ region of the spectrum is comprised of overlapping signals from Fe^{3+} sites affected differently by the dehydration process leading to a distribution of ZFS parameters. In order to further study the origin of the observed changes in the ESR spectrum and to investigate the consequences of dehydration on the local environment of the Fe^{3+}, ED-ESR and ESEEM experiments were performed on the hydrated, dehydrated, and rehydrated samples.

ED-ESR Measurements. The ED-ESR spectra of the as-synthesized and dehydrated FeFAU2 samples are shown in Figure 7B. Since strong ^{27}Al modulation and weak ^1H modulation were observed on the echo decay envelope of FeFAU2, the ED-ESR spectra shown in Figure 7B were recorded with a large τ value ($\tau = 1.5$ μs) at which time most of the modulation had decayed away. While the $g = 4.3$ signal intensity is very weak in the ED-ESR spectra recorded at long τ values, its intensity is larger

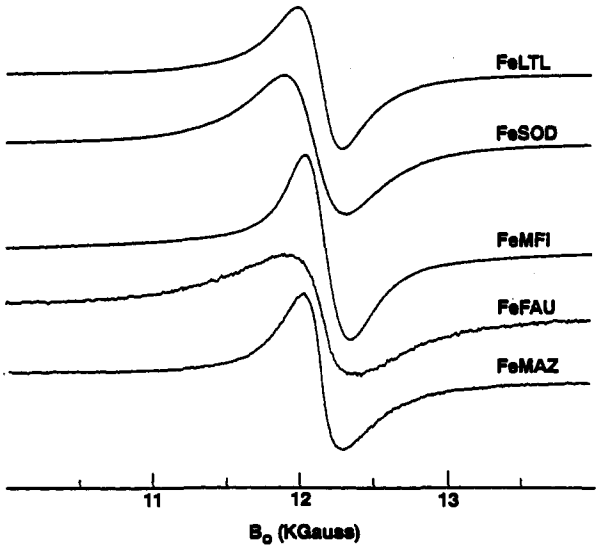

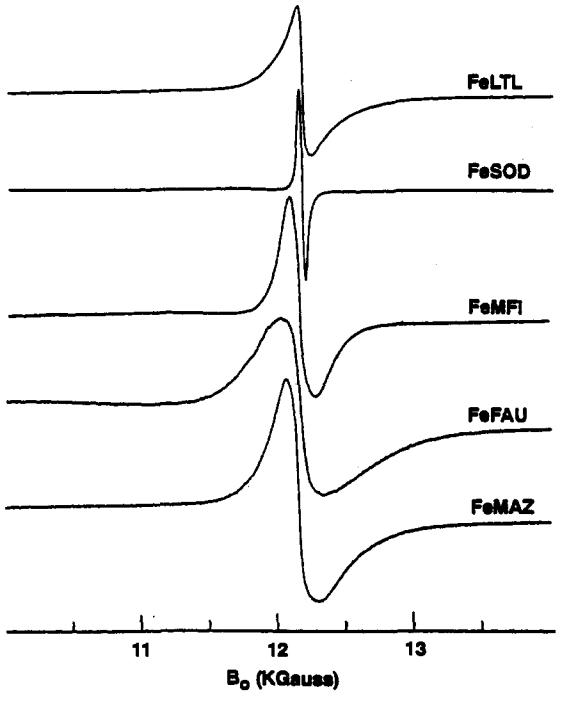

Figure 3. Q-band ESR spectra recorded at room temperature of (A, top) the high-level Fe content zeolites FeLTL2, FeSOD2, FeMFI2, FeFAU4, and FeMAZ2 and (B, bottom) the low-level Fe zeolites FeLTL1, FeSOD1, FeMFI1, FeFAU2, and FeMAZ1.

Table 2. Line Width,[a] ΔB, of the $g = 2$ Signal in X- and Q-Band Spectra for the High and Low Fe Content Zeolites Studied

zeolite	ΔB (G), RT X-band high Fe	ΔB (G), RT Q-band high Fe	ΔB(X)/ ΔB(Q)	ΔB (G) 140 K X-band low Fe	ΔB (G), RT, Q-band low Fe	ΔB(X)/ ΔB(Q)
FeLTL	328	291	1.13	234	97	2.41
FeSOD	454	405	1.12	156	46.2	3.39
FeMFI	501	300	1.67	344	185	1.86
FeFAU	688	450	1.53	391	291	1.34
FeMAZ	422	300	1.41	344	228	1.50

[a] Measured from the peak to peak distance in the derivative spectrum.

in the ED-ESR spectrum recorded with $\tau = 0.19$ μs (see Figure 8B). This indicates that the T_m for the $g = 4.3$ signal is significantly shorter than that of the $g = 2$ signal.

The integrated ESR spectra, shown in Figure 9, of the as-synthesized and dehydrated (398 K) samples facilitates comparison of the ESR relative intensities with those of the ED-ESR spectra appearing in Figure 8B. The integrals of the ESR spectra

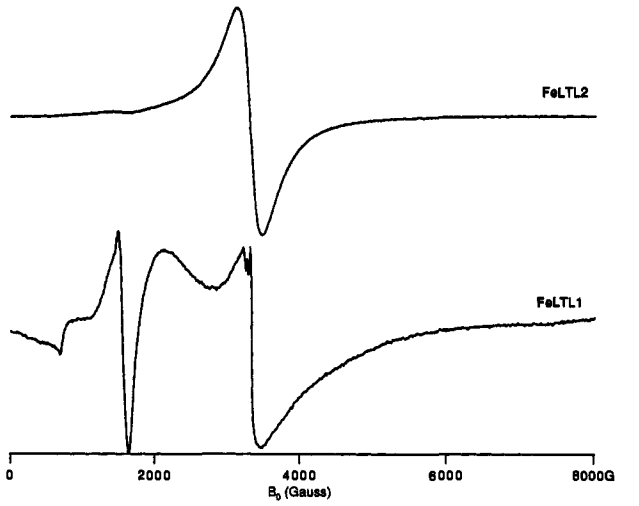

Figure 4. X-Band ESR spectra (RT) of FeLTL2 (6.6% Fe) and FeLTL1 (0.07% Fe).

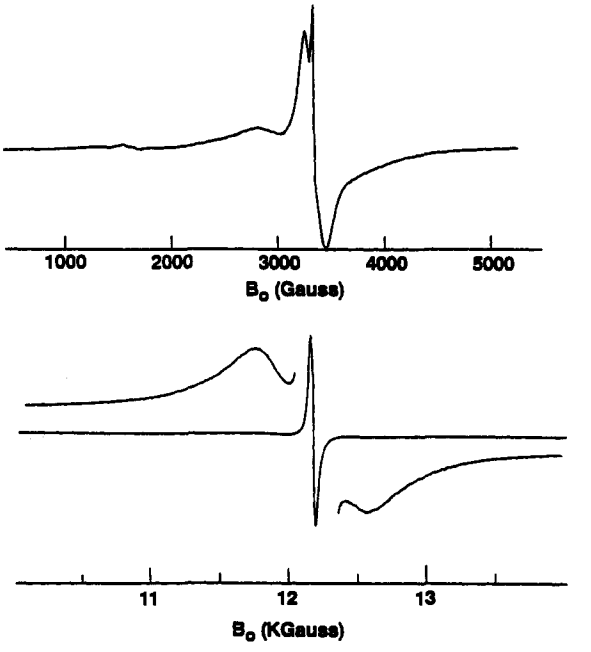

Figure 5. X-Band ESR spectrum of FeSOD1 (RT) (A, top), and its Q-band spectrum (RT) (B, bottom). The inset is a vertical expansion of the outer wings.

are in satisfactory agreement with the corresponding ED-ESR spectra although in the latter the $g = 4.3$ signal is relatively weaker, consistent with the relaxation "contrast" effect discussed earlier. Both types of spectra show that the majority of the ESR signal arises from the broad line centered at $g = 2$. Unfortunately, the intensities of the signals cannot be simply related to the relative concentration of the Fe^{3+} sites yielding these signals because careful consideration is needed of the transition probabilities involved.[26] Nonetheless, the overwhelmingly stronger intensity of the $g = 2$ signal does suggest that it accounts for a significant fraction of the Fe.

Rehydration of the FeFAU2 sample dehydrated at 398 K regenerated the original ESR spectrum whereas rehydration of the sample dehydrated at 673 K resulted in a significantly different ESR spectrum as shown in Figure 8A. The broad signal at $g \approx 2.3$ dominates the spectrum of the rehydrated sample and it appears that the intensity of the $g = 2$ signal is reduced with respect to the $g = 4.3$ signal. In contrast to the changes observed in the ESR spectra, the ED-ESR spectra, shown in Figure 8B, of the as-synthesized and rehydrated samples are virtually indistinguishable. This suggests that the Fe^{3+} species at $g \approx 2.3$

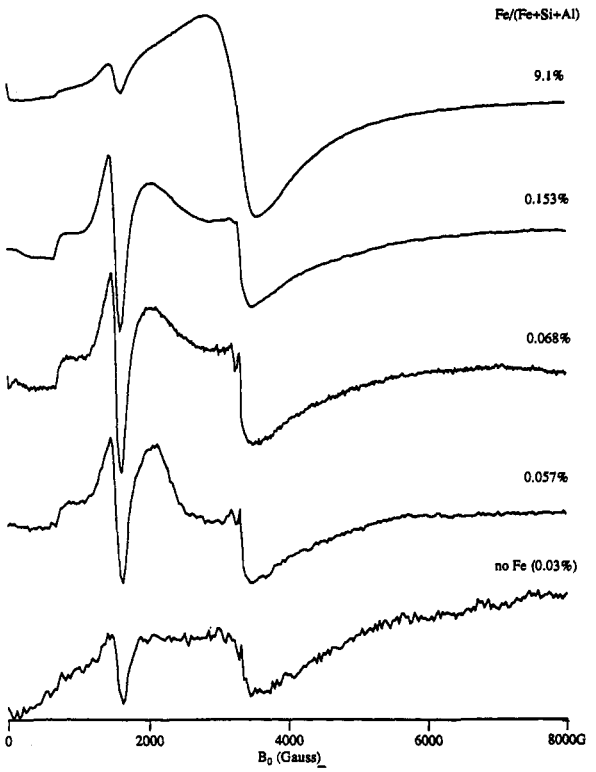

Figure 6. X-Band ESR spectra (140 K) of FeFAU as a function of the Fe content (samples FeFAU0–4).

does not contribute to the echo most likely due to a strong spin–spin interaction leading to short (T_m and/or T_1) relaxation times. Therefore, we assign this signal to "aggregated" Fe^{3+} generated by the high-temperature dehydration followed by rehydration. The formation of such Fe^{3+} aggregates within the zeolite cavities likely involves as a first step the hydroxylation of framework Fe^{3+} at high temperature. This is analogous to the dealumination process used to manufacture "ultrastable" faujasite.[52]

ESEEM Measurements. Figure 10 shows the two-pulse Fourier transform (FT) ESEEM spectra of FeFAU2 as a function of the external magnetic field within the ESR spectrum. As B_0 increases, the modulation amplitude of all ESEEM lines decreases. This is expected, since the modulation amplitude is a function of the probabilities of the forbidden ESR transitions, which in turn are inversely proportional to the magnetic field.

The ESEEM spectra in Figure 10 contain several peaks (identified in the figure) assigned as follows: $\nu_L(Al)$, $2\nu_L(Al)$, $\nu_L(H) - \nu_l(Al)$, $\nu_L(H)$, $\nu_L(H) + \nu_l(Al)$, and $2\nu_L(H)$, where $\nu_L(Al)$ and $\nu_L(H)$ correspond to the Larmor frequency of the ^{27}Al and ^1H nuclei, respectively. At 1370 G the ESEEM peaks appear at 1.47, 3.0, 4.41, 5.98, 7.35, and 12.0 MHz, respectively. The frequency shift of the peak positions as a function of the external magnetic field is as expected for their Larmor frequencies and confirms their assignments. In principle it is possible that the ESEEM peaks assigned to ^{27}Al could also arise from ^{23}Na cations, since it is difficult to distinguish their Larmor frequencies at those low magnetic fields. This possibility is however excluded, since the ESEEM of FeFAU2 exchanged with K^+ gave similar ESEEM wave forms.

The negative amplitude of $2\nu_L(H)$ is characteristic of the combination harmonic ($\nu_\alpha + \nu_\beta$) typically appearing in the two-pulse FT-ESEEM spectra. A similar negative peak due to the ^{27}Al combination harmonic is evident only at fields above 1800 G. The other combination harmonics have positive amplitudes and originate from the hyperfine interaction with two or more interacting nuclei.[30,45] Note that the two combination peaks centered about the proton Larmor frequency can easily be misinterpreted as a proton hyperfine doublet originating from a strongly coupled proton(s). It is the field dependence of the "doublet" line width and splitting that cannot be accounted for, even by assuming a large hyperfine anisotropy, thus excluding its assignment as a hyperfine doublet. This example demonstrates that when deep modulation and several nuclei are involved in the modulation, combination lines are likely to be observed. In this case, measuring the magnetic field dependence of the ESEEM lines is essential in order to corroborate line assignments.

As a probe of the variation in the local environment of the Fe^{3+} sites, we have compared the modulation patterns of the as-synthesized FeFAU2 with that of the sample that was dehydrated at 673 K and then rehydrated. The ESEEM patterns were recorded for all samples under identical conditions and were compared through the ratio method.[46]

The echo intensity can be represented as a product of two functions:

$$V(\tau;T) = F_{mod}(\tau;T)\, F_{decay}(\tau;T)$$

The modulation effect is included in $F_{mod}(\tau;T)$ whereas the relaxation is given by $F_{decay}(\tau;T)$. Modulation patterns can be considered identical if their ratioed wave forms contain no residual modulation. In this case the ratioed wave form is given by the ratio of the decay functions which may not necessarily be the same for the two samples.

Figure 11A shows the ratios of the three-pulse ESEEM wave forms of FeFAU2 before and after a dehydration/rehydration cycle as a function of the magnetic field within the ESR spectrum. In these experiments τ was adjusted at each field to optimize the ^{27}Al and ^1H modulation. While no modulation was observed in the ratios of the ESEEM wave forms recorded down to 2600 G, significant modulation was detected at fields below this value, as shown in Figure 11A. The FTs of the ratioed ESEEM wave forms recorded at these lower field values are shown in Figure 11B. At 1370 G both ^{27}Al and strong ^1H modulation are evident. The proton modulation has comparable amplitudes in the FT-ESEEM spectra recorded at 1370 and 1570 G, yet it is significant stronger in the FTs of the ratioed ESEEM wave forms obtained at 1370 G. In all fields where a difference in the modulation amplitude was observed, it was always stronger in the as-synthesized sample.

From these ESEEM experiments we conclude that the dehydration at 673 K caused a change in the immediate environment of the Fe^{3+} sites that give rise to the low-field ESR signals. The "new" surroundings have fewer protons (belonging to water or hydroxyl group ligands) and a shallower Al modulation. The latter can be caused by one of the following: an irreversible change in the quadrupole interaction for some fraction of the ^{27}Al in the zeolite framework, a change in the number of ^{27}Al atoms interacting with the Fe^{3+}, or a change in the distance between the Fe^{3+} and ^{27}Al. Unfortunately, a more quantitative analysis of the origin of the change in the ESEEM intensities is prohibitive because of the large number of unknown magnetic parameters required to simulate the spectra.

Discussion

Evidence for the presence of framework Fe^{3+} sites in FeSOD2 and FeLTL2 was obtained from both our UV–vis results and chemical analysis. Peaks in the UV–vis spectrum are characteristic of Fe^{3+} in a tetrahedral environment, and the chemical analysis showed that the amount of charge-balancing cations corresponds to the sum of the Fe and Al content. Further support for the presence of framework Fe in these zeolites was obtained from previous anomalous dispersion EXAFS studies of FeLTL[8] and FeSOD[9] samples which had ESR spectra similar to those used in the present study. In those studies Fe was assigned to framework sites based on the distance to four oxygens in the first coordination shell and an outer shell of silicon. Since the ESR

(52) Scherzer, J. ACS Symp. Ser. **1984**, *248*, Chapter 10.

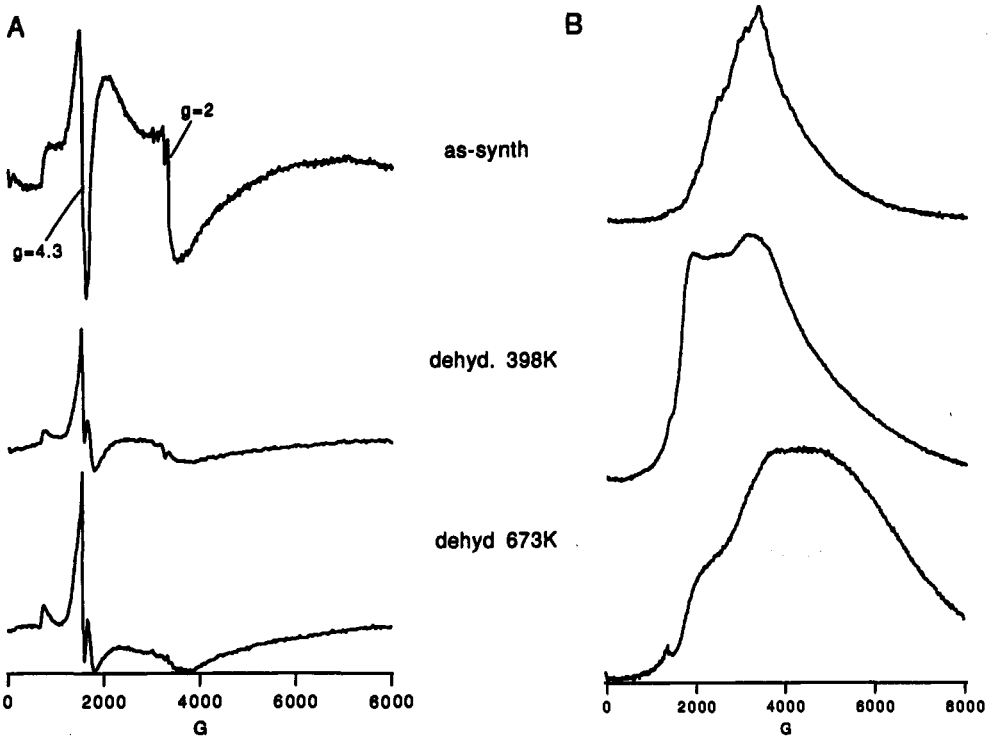

Figure 7. (A) X-Band ESR spectra (140 K) of FeFAU2 before and after dehydration at 398 and 673 K as indicated. (B) ED-ESR spectra of the same samples recorded at 1.2 K with τ = 1.5 μs.

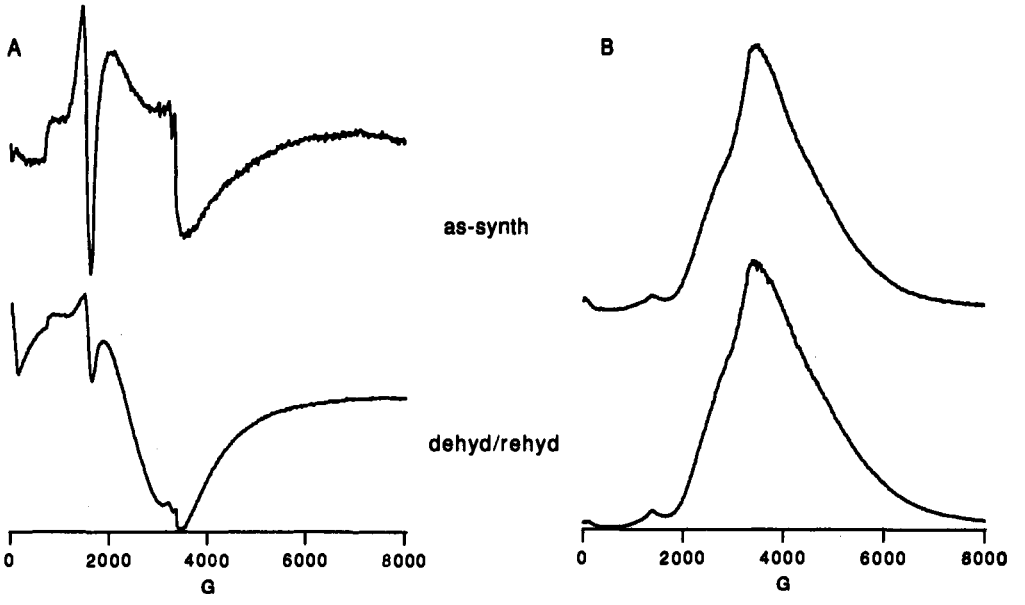

Figure 8. (A) X-Band ESR spectra (140 K) of as-synthesized FeFAU2 before and after dehydration at 673 K and rehydration. (B) ED-ESR spectra of the same samples recorded at 1.2 K and τ = 0.19 μs.

g = 4.3 signal is absent in FeSOD2 and in FeLTL2 its relative intensity is negligible, we unambiguously conclude that framework Fe in zeolites does not necessarily have an exclusive signal at g = 4.3 but may have a g = 2 signal.

This assignment is in agreement with that of Fe in FeMFI by Lin *et al.*[6] Our results, however, do not agree with the original assignment of McNicol *et al.*,[1] who assigned the g = 4.3 peak to framework Fe^{3+} in NH_4^+ faujasite and NH_4^+ mordenite. Phosphorescence measurements were reported to unambiguously determine the existence of tetrahedral Fe^{3+} in both zeolites. The optical measurements in conjunction with the invariance of the Fe content in NaY and Na-mordenite toward ion exchange with NH_4Cl, the similarity of the ESR spectrum of the Na^+ and NH_4^+ forms, along with the appearance of a g = 4.3 signal in silica[1] led to the assignment of the g = 4.3 signal to framework Fe. McNicol *et al.*,[1] however, did not discuss why the broader signal appearing at g = 2 should be excluded from assignment to framework Fe.

The g = 4.3 signal in the spectrum of silica was assigned to Fe in the framework sites with a nonbridging oxygen to account for the low symmetry caused by two charges "attached" to two of the oxygens.[25] By analogy, the g = 4.3 signal in the zeolite can be assigned to Fe framework "defect" sites, with terminal oxygens. This may explain the difference in the spectra of high- and low-level FeLTL. The amount of "defect" sites are normally small compared to the total number of tetrahedral (known as "T") sites. Assuming that the Fe^{3+} has a larger affinity to these sites, at low Fe contents, they will comprise a significant amount of the Fe framework sites, whereas at high Fe contents, after being saturated, their relative contribution to the ESR spectrum will decrease. Accordingly, the lack of this signal in FeSOD1 suggests that the number of these "defects" in FeSOD is negligible. This hypothesis can be verified by looking for a correlation between the intensity of the g = 4.3 signal and the amount of terminal OH. We note, however, that extraframework Fe^{3+} cations can

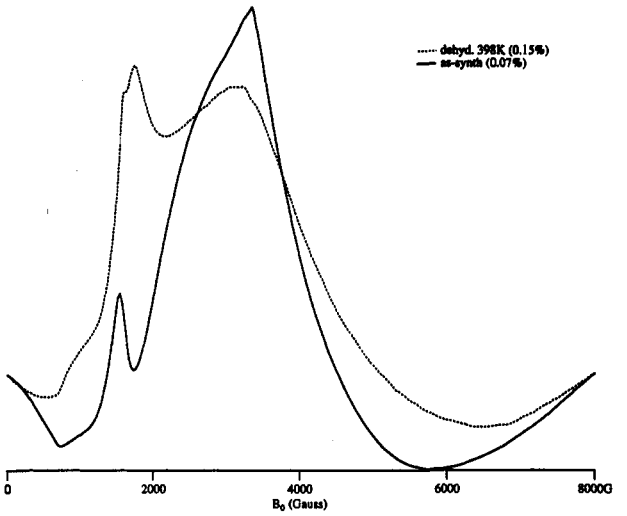

Figure 9. Integrated X-band ESR spectra of FeFAU3 and FeFAU2 dehydrated at 398 K.

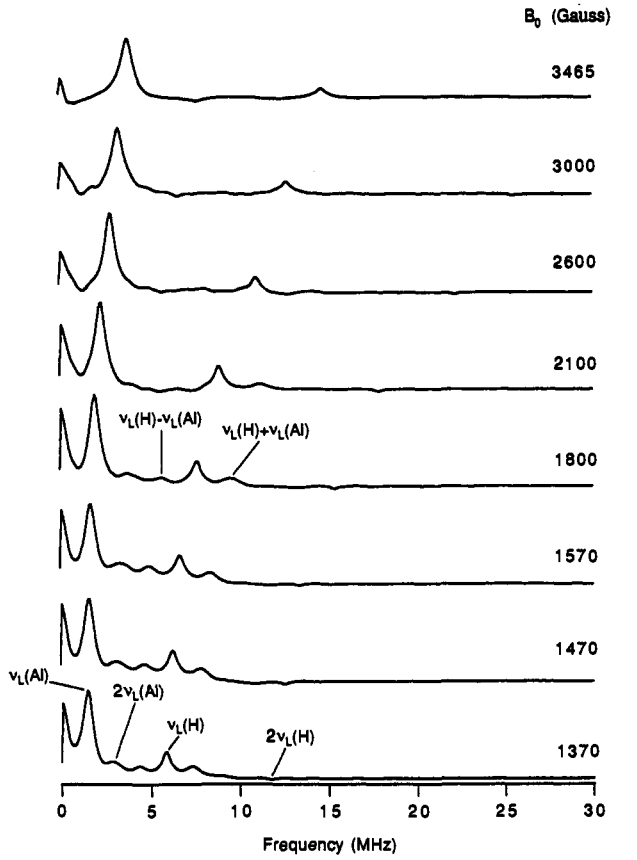

Figure 10. Two-pulse Cosine FT-ESEEM spectra of FeFAU2 recorded at 1.2 K as a function of the resonant magnetic field.

also give rise to a $g = 4.3$ signal, as we observed in Fe^{3+}-exchanged NaY.

The assignment of framework Fe in FeSOD and FeLTL to the $g = 2$ signal does not exclude the possibility that extraframework Fe^{3+} in a rather highly symmetrical environmental would also yield a $g = 2$ signal. In fact such a possibility is highly probable, as indicated by the exchanged Fe^{3+} FeLTL spectrum. Further support for this possibility is obtained from the comparison of the $g = 2$ line width in the X- and Q-band spectra of the low-level Fe zeolites we investigated. Only in the FeSOD1 could the broadening be fully attributed to the ZFS. In all other samples there are other sources of broadening, one of which could be overlapping signals of different species. While sodalite and faujasite have only one type of T site, L and mazzite have two different T sites, and MFI has 12 different T sites. In principle,

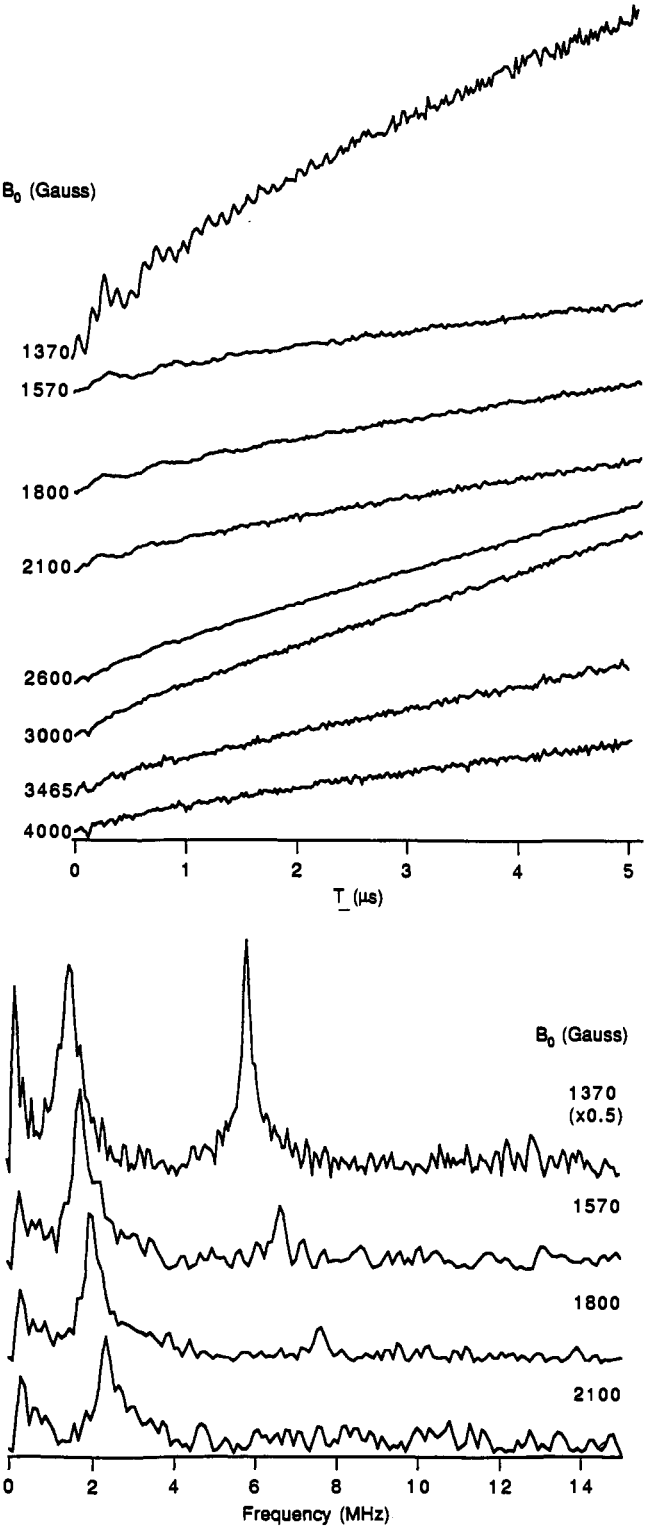

Figure 11. (A, top) Ratios of the three-pulse ESEEM of as-synthesized FeFAU2 and FeFAU after dehydration at 673 K and rehydration. The τ values from bottom to top are 0.16, 0.16, 0.21, 0.24, 0.18, 0.21, 0.24, and 0.27 μs. (B, bottom) The corresponding Fourier transforms of the low-field ratios (magnitude spectra).

Fe^{3+} can occupy any of these sites. Each site may have slight different ZFS contributing to the inhomogeneity in the spectrum. The ESR results, however, are not sensitive enough to detect the subtle differences between such sites, and for all practical considerations, the spectra of FeMAZ, FeFAU, and FeMFI are very similar.

In a series of single-crystal experiments on Fe^{3+} sites in α-quartz, Weil and co-workers determined both the g (which exhibits extremely small anisotropy) and ZFS tensors.[47-51] They were able to deduce the location of Fe^{3+} substitutional sites from the

direction of both the g-tensor and the ZFS tensors with respect to the bond orientation. In orientationally disordered systems of high-spin Fe^{3+}, the extremely small g-anisotropy cannot be detected and is therefore assumed to be isotropic. Accordingly, structural information regarding the Fe^{3+} site in powders is contained in the ZFS tensor. Under the best circumstances, analysis of the ESR powder pattern can yield D and E. These values can be further interpreted for the case of $g\beta B_0 \gg |D,E|$ as axial or nonaxial deviations from octahedral or tetrahedral symmetries. Nevertheless, the powder ESR spectrum does provide information regarding the different types of Fe^{3+} sites present.

The FeFAU seems to contain a significant amount of nonframework Fe, as indicated by its tan color, characteristic of ferric hydroxide. The chemical analysis however strongly suggests that framework Fe exists as well, since [Na]/([Al] + [Fe]) ≈ 1 (see FeFAU4, Table 1). Combined ESR and ED-ESR spectroscopy detected in FeFAU the formation of aggregates of extraframework Fe^{3+} as a consequence of dehydration at 673 K followed by rehydration. These aggregates could be generated either by migration of extraframework Fe^{3+} species or by dislodging Fe^{3+} from the framework by hydrolysis at high temperature in the presence of residual water. This may involve the formation of pentahedral Fe^{3+} analogous to what has been observed for Al^{3+} in aluminosilicates and P^{5+} in aluminophosphates.[53] At high enough temperatures, dehydration can also cause partial reduction to ferrous iron along with dehydroxylation. Subsequent rehydration, which generates the intense $g = 2.3$ signal, may generate particles of ferric oxides which do not contribute to the echo. Fe^{3+} dislodged from the framework can also become incorporated into these particles in analogy to the formation of aluminum oxide in dealuminated zeolites.[52] This assignment of the $g \approx 2.3$ signal is in agreement with previous assignments,[1,2] but in disagreement with Lin *et al.*,[6] who attributed the 2.3 signal in FeMFI to tricoordinated framework Fe. There, however, the ESR spectrum was reversible after dehydration at 773 K followed by rehydration.

The broadening of the $g = 2$ signal of FeFAU upon dehydration is consistent with the assignment of framework Fe^{3+} to this signal whereby the dehydration induces significant framework distortions leading to an increase in D and E. Evidence for such distortions has been previously detected by excessive broadening of the NMR spectra of ^{27}Al in dehydrated zeolites due to the increase in the quadrupole interaction,[54] and in ESEEM spectra where the ^{27}Al modulation depth decreases significantly for the same reason.[55] We note though that extraframework Fe^{3+} can also experience an increase in D due to the dehydration process.

Any Fe^{3+} which undergoes reversible changes under the dehydration/hydration cycle should have magnetic interactions with ^{27}Al which are invariant to this hydrothermal treatment process. Hence, framework Fe^{3+} which was not disloged by the high-temperature dehydration is expected to show the same ^{27}Al modulation in the ESEEM experiment before and after the dehydration/hydration cycle. The experimental results show that while no changes were detected in the ESEEM recorded around $g = 2$, significant differences were observed in both the ^{27}Al and ^{1}H modulation depth for ESEEM obtained in the $g = 4.3$ region. Although changes were observed in the ESEEM experiment, the dehydration/hydration cycle had insignificant effects on the ED-ESR, demonstrating the better sensitivity of ratioed ESEEM to subtle changes in the local environment. Differences in the modulation can be due to the generation of Fe^{3+} sites with similar ED-ESR spectra but with different arrangements of ^{27}Al and ^{1}H nuclei in the vicinity of the Fe^{3+}, giving rise to different ESEEM intensities. For instance, the abstraction of a water molecule from a ferric hydroxide and a nearby terminal Si–OH can form an isolated Fe^{3+} coordinated to the surface (internal or external) oxygen, generating a Fe–O–Si site. This site would be further away from framework ^{27}Al, resulting in a reduced ^{27}Al modulation depth while the loss of a net number of nearby protons would decrease the proton modulation amplitude.

Finally we discuss the possibilities that the $g = 2$ signal may be due to low-spin Fe^{3+} or due to high-spin Fe^{2+}. First, we note that the anisotropy of the g-factor for low-spin Fe^{3+} is much larger than observed.[22] Second, in the pulsed ESR experiments a lower transmitter power than normally employed in experiments for $S = {}^1/_2$ systems was used to achieve an effective $\pi/2$ pulse. This is consistent with the higher nutation frequency expected for $S > {}^1/_2$.[56] Third, a low-spin multiplicity is unlikely, since possible Fe^{3+} ligands (water, hydroxyl, and framework oxygen) are not strong field ligands which would lead to low-spin Fe^{3+}. Furthermore, we exclude the possibility of the presence of Fe^{2+} in as-synthesized samples on the basis of chemical arguments. Iron is introduced in the ferric form, and the synthesis conditions should not lead to reduction. Fe^{2+} could be generated as a consequence of dehydration.[17] However the integer spin ESR signals for high-spin Fe^{2+} are only observed at low temperature (liquid He range) and appear at high g values and not at $g = 2$.[22]

Conclusions

The ESR spectral properties of high-spin Fe^{3+} in polycrystalline zeolites are dominated by the zero field splitting parameters, D and E. These parameters are not *uniquely* correlated to the chemical structure of the Fe^{3+} site. Therefore the ESR data must be combined with other physical and/or chemical methods. From our combined X- and Q-band ESR, ED-ESR, ESEEM, UV–vis, and chemical analysis results in conjunction with previously reported EXAFS,[8,9] data, we conclude that (1) Fe^{3+} can be incorporated into framework sites in significant amounts in FeSOD, FeLTL, FeMFI, and FeMAZ and likely also in FeFAU. In each case framework Fe^{3+} exhibits a $g = 2$ ESR signal. (2) Extraframework Fe^{3+} can also show a $g = 2$ signal. Therefore the appearance of the $g = 2$ signal in zeolites does not provide evidence for framework substitution unless combined with other physical or chemical methods. (3) The absence of the $g = 4.3$ signal in the ESR spectrum does not exclude the possibility of framework substitution in zeolites. Moreover, the appearance of the $g = 4.3$ signal does not by itself necessarily indicate framework location. (4) FeSOD with low Fe loadings has a single Fe^{3+} site exhibiting a unique narrow $g = 2$ signal. It can therefore serve as a good model for further studies of Fe substitutions in zeolites. (5) FeFAU contains a rather large amount of extraframework Fe. Dehydration/rehydration cycling produces phases with "aggregates" of Fe ions generated either by dislodged framework Fe^{3+} and/or by migration of extraframework Fe^{3+}.

Acknowledgment. We thank Dr. D. van Ormondt for providing us with the LPSVD computer program.

(53) Gilson, J.-P.; Edwards, G. C.; Peters, A. W.; Rajagopalan, K.; Wormsbecher, R. F.; Roberie, T. G.; Shatlock, M. P. *J. Chem. Soc., Chem. Commun.* **1987**, 91.
(54) Luz, Z.; Vega, A. J. *J. Phys. Chem.* **1986**, *91*, 374.
(55) Goldfarb, D.; Kevan, L. *J. Magn. Reson.* **1989**, *82*, 270.
(56) Isoya, J.; Kanda, H.; Norris, J. R.; Tang, J.; Bowman, M. K. *Phys. Rev. B* **1990**, *41*, 3905.